Hydrocracking of Coconut Oil on the NiO/Silica-Rich Zeolite Synthesized Using a Quaternary Ammonium Surfactant

Sriatun[1,2*], Heru Susanto[3], Widayat[3], and Adi Darmawan[2]

[1]*Chemical Engineering Doctoral Programme, Faculty of Engineering, Diponegoro University, Jl. Prof. Soedharto SH, Tembalang, Semarang 50275, Indonesia*

[2]*Department of Chemistry, Faculty of Science and Mathematics, Diponegoro University, Jl. Prof. Soedharto SH, Tembalang, Semarang 50275, Indonesia*

[3]*Department of Chemical Engineering, Faculty of Engineering, Diponegoro University, Jl. Prof. Soedharto SH, Tembalang, Semarang 50275, Indonesia*

** **Corresponding author:***

tel: +62-85100127747
email: sriatun@live.undip.ac.id

Received: April 18, 2020
Accepted: August 7, 2020

DOI: 10.22146/ijc.55522

Abstract: *NiO/silica-rich zeolite catalysts were used for coconut oil hydrocracking. The catalyst consists of a mixture of Na_2SiO_3, $Al(OH)_3$, NaOH, and quaternary ammonium surfactants. The surfactant was varied of types like as tetrapropylammonium bromide (TPAB) and cetyltrimethylammonium bromide (CTAB). The acidity of the silica-rich sodalite zeolites enhances with the increase in nickel oxide added through a wet impregnation. The hydrocracking process was carried out by a semi-batch method. Liquid products were analyzed using GC-MS. The results showed that the addition of surfactants increased the catalyst surface area and acidity. Meanwhile, the presence of nickel oxide increases the acidity of the catalyst. The hydrocracking results showed an increase in gas products when the surface area was high, i.e., 23.781% in silica-rich sodalite zeolite without template (Z), 32.68% in silica-rich sodalite zeolite with tetrapropylammonium (ZTPA), and 39.673% in silica-rich sodalite zeolite with cetyltrimethylammonium (ZCTA). The presence of NiO increased the liquid product and the selectivity of the bioavtur fraction (C_{10}-C_{15}), where the highest percentage of liquid product was 60.07% at NiO/ZTPA.*

Keywords: *hydrocracking; coconut oil; NiO; silica-rich zeolite; sodalite; quaternary ammonium surfactant*

■ INTRODUCTION

The most common zeolite in the zeolite mineral group is the sodalite mineral (SOD). The chemical composition of sodalite is $Na_6(Si_6Al_6O_{24})\cdot H_2O$. A sodalite is a host material (host molecule) that is important in forming simple crystal structures of various synthetic zeolites. Sodalite zeolite has a cubic crystal structure. The structure formed by the β-cage framework consists of eight six-member rings in which alternates between the SiO_4 and AlO_4 tetrahedral, and the α-cage consists of six four-membered rings [1]. As the Si concentration in the reactant mixture or the Si/Al ratio increases, the size, and shape of the crystals change, in which the octahedral and dodecahedral framework in the zeolite's internal structure become dominant [2].

The study of the synthesis of sodalite zeolites has been carried out by Dey et al. [3], who synthesized silica-rich sodalite by adding a trioxane template. The results indicated that trioxane has a strong structural directing or templating effect on the SOD structure. At Si/Al ratios lower than 20, another product was obtained, whereas, at very low temperatures or short synthesis times, the resulting product was still amorphous. Another study has reported zeolite-Y synthesis that successfully used surfactants as templates with the hydrothermal method for 72 h [4]. In another study, CTAB as a structural directive in zeolite synthesis has also been used at

various Si/Al ratios with a hydrothermal temperature of 100 °C for three days. The results indicated that the Si/Al ratio influences the size and shape of zeolite granules/crystals. The use of a CTAB surfactant as a directing agent improves the crystallinity of zeolites and influences the size and homogeneity of zeolite particles [5]. Neutral surfactants such as PEG and cationic surfactants such as CTAB have an important role in the formation of zeolite crystals [6]. Other studies have been reported for LTA type silica-rich zeolite with Si/Al ratio = 17 using tetramethylammonium and 1,2-dimethyl-3-(4-methyl benzyl) imidazolium as templates [7]. Large amounts of Si in the framework cause more durable hydrophobic properties, higher acidity, and greater surface area [8]. These properties satisfy the conditions for this material to be used in reactions that require high temperatures, such as the hydrocracking process. Also, principles of "like dissolves like" can be fulfilled when hydrophobic materials as catalysts interact with nonpolar/hydrophobic feeds and coconut oil. Previous studies concluded that the Si/Al ratio and the use of templates were very influential on the zeolite characters [9-11].

The use of zeolite from bagasse ash as a catalyst in biodiesel production from used cooking oil through the transesterification reaction has also been carried out. Transesterification results showed that at a ratio of methanol: oil of 1:3 for 60 min, 13.83% of Methyl Ester (MES) products were produced, consisting of methyl caprylate, methyl caprate, methyl laurate, methyl myristate, methyl palmitate, methyl linoleate, and methyl stearate. In the methanol: oil ratio of 6:1, the biodiesel obtained was 85.51%, with methyl caprate as the main component [12]. NiO and CoO-supported halloysite nanotubes have also been used as catalysts for hydrocracking of the heavy oil residues. The hydrocracking process was carried out at a temperature of 450 °C with varying H_2 pressures ranging from 1–4 MPa. The results showed an increase in liquid products consisting of gasoline and diesel from 52 to 57% when the pressure rose from 1 to 4 MPa [13]. This information showed that zeolite has excellent performance as a catalyst.

Biofuel can be produced from renewable materials or biomass through several processes such as catalytic cracking, hydrocracking or deoxygenation of vegetable oils containing triglycerides, Fischer-Tropsch process in the synthesis of bio-origin fuels [14-16], from virgin coconut oil waste [17], and marine biofuel from lignocellulose [18]. Castor oil hydroprocessing was promoted by nickel-based bifunctional catalysts to produce bio-jet fuels (bioavtur) [19]. Widiyadi et al. [20] had carried out the hydrocracking process using $NiMo/Al_2O_3$ catalyst on dirty palm oil to produce biokerosene. Besides, the hydrocracking process was carried out using a sulfided $NiMo/Al_2O_3$ catalyst to produce bio-jet fuel (bioavtur) from natural triglycerides/coconut oil. The operating conditions of the process were at temperature of 280–380 °C, the pressure of 30 bar, liquid hourly space velocity (LHSV) of 1.0–3.0/h, and H_2/feed volume ratio of 600 Nm^3/m^3) [21]. Meanwhile, Al-Muttaqii et al. [22] and Widayat et al. [23] have produced biokerosene and biofuel from coconut oil using a Ni-Fe/HZSM-5 and Zn/HZSM-5 catalyst through a hydrocracking process.

Coconut oil is a renewable material and can be used as a raw material for biofuel production. Coconut plants are easy to grow and suitable for the Indonesian climate. Therefore, their availability can be maintained. Coconut oil is easily found on the market at a relatively low price. According to Boateng et al. [24], the largest components of coconut oil are lauric acid (49%) and myristic acid (18%). The most important reason for using coconut oil for hydrocracking is as coconut oil contains a high compound of C_{10}–C_{16}, thus providing an opportunity to be converted to hydrocarbons with the same amount of carbon or cracked into hydrocarbons with smaller amounts of carbon.

There has been no report on the use of templates to synthesize silica-rich sodalite. The use of sodalite, a simple structure of the zeolite, has not been reported as a catalyst in the hydrocracking reaction of coconut oil. As the presence of a template of quaternary ammonium surfactant increases surface area and uniformity [25], this research studies the effect of quaternary ammonium surfactant templates on the structure of silica-rich

sodalite zeolites. The choice of cetyltrimethylammonium and tetrapropylammonium bromide surfactants is expected to provide a significant pore size difference. The research also studies the effect of adding NiO in silica-rich zeolites. Ni or NiO metal dispersion to sodalite-rich zeolite silica is expected to increase the acidity and surface area of the material so that the active catalytic site also rises. All materials were tested for their catalytic ability to convert coconut oil into biofuels through a hydrocracking reaction. Catalysts with many active sites are expected to improve hydrocracking products and selectivity.

■ EXPERIMENTAL SECTION

Materials

All chemicals used in this study are analytical grades. The chemicals from Merck were sodium hydroxide (NaOH) 98%, sodium silicate (Na_2SiO_3, 27% SiO_2), cetyltrimethylammonium bromide (CTAB) 98%, nickel(II) nitrate hexahydrate ($Ni(NO_3)_2{\cdot}6H_2O$) 99%, hydrofluoric acid (HF) 48%, ammonia (NH_4OH) 25%, hydrochloric acid (HCl) 37%. Meanwhile, the chemicals from Sigma Aldrich were aluminum hydroxide ($Al(OH)_3$, 50–57% Al_2O_3), and tetrapropylammonium bromide (TPAB) 98%. The hydrocracking process used coconut oil which was purchased from a supermarket in Semarang, Indonesia.

Instrumentation

The crystallinity of synthesized catalysts was characterized using an X-ray diffractometer (XRD) (Bruker D2 Phaser 2nd Gen) with Cu Kα radiation, the wavelength of 1.54060 Å, and under the setting of 30 kV and 10 mA. Determination of the surface and pore parameter of the synthesized catalysts was performed using a Gas Sorption Analyzer (GSA) (Quantachrome NovaWin) with sample weight: 0.1129 g, outgas time: 3.0 h, analysis gas: nitrogen, analysis time: 133.3 min, Cell ID: 4, outgas temp: 300 °C, bath temp: 77.3 °K. The surface area was determined by a multi-point Brunauer-Emmett-Teller (BET). The estimation of total pore volume and the distribution of pore size was conducted by the desorption isotherms of the Barret-Joyner-Halenda (BJH) method. The functional groups of the synthesized catalysts after adsorbing ammonia gas were determined using a Fourier-transform infrared (FTIR) Spectrometer (PerkinElmer Spectrum Version 10.03.06) with the KBr method. Meanwhile, the composition of the liquid product from hydrocracking was identified using GCMS (QP2010S SHIMADZU with column type: Rtx 5 MS, ID: 0.25 mm, carrier gas: Helium, Ionizing: EI 70 Ev, Column temperature: 40 °C, Injection temperature: 310 °C, Injection mode: split, Column flow: 0.57 mL/min).

Procedure

Synthesis of catalyst

An amount of 5.6 g of NaOH was dissolved in 20.7 mL of H_2O and heated until all of the NaOH dissolved. It was subsequently added with 0.45 g of $Al(OH)_3$ until fully dissolved to give a sodium aluminate solution. The solution was reacted with 16.33 mL of Na_2SiO_3 solution and stirred at room temperature until the mixture thickened. The mixture was transferred into a Teflon container for the hydrothermal process and heated at 200 °C for 24 h in an autoclave. The product was then washed with distilled water until it reached pH ± 7, and after that, it was dried in an oven at 100 °C for 2 h. This product code was Z.

ZTPA was produced using a TPAB surfactant template, in which 3.328 g of TPAB was dissolved in 25 mL of H_2O, then added to sodium aluminate and stirred until homogeneous. The mixture was added with a 16.33 mL of Na_2SiO_3 solution. The hydrothermal process was carried out at 200 °C for 24 h in an autoclave. The resulting product was washed until a neutral pH obtained (± 7), and after that, it was dried. The solid product was calcined at 550 °C for 3 h to remove the template. The same procedure was applied to synthesize ZCTA using a 4.554 g of CTAB surfactant. Both products were characterized by XRD and GSA techniques.

The NiO/silica-rich zeolite catalysts were prepared by incipient wetness impregnation. Several silica-rich zeolites were impregnated with aqueous solution of nickel(II) nitrate hexahydrate ($Ni(NO_3)_2{\cdot}6H_2O$) to contain 3% (weight) of nickel. The mixture was stirred at 30 °C for 24 h and evaporated at 90 °C until the paste was formed. Then the paste was dried at 110 °C and

calcined at 550 °C for 3 h. This process aimed to form NiO from Ni^{2+} ions. The impregnation products were NiO/Z, NiO/ZTPA, and NiO/ZCTA, each of which refers to a catalyst without a template, tetrapropylammonium-templated catalyst and the cetyltrimethylammonium-templated catalyst, respectively. Afterward, the catalysts obtained were characterized using GSA.

The catalyst's total acidity was determined using the gravimetric method with ammonia gas as an adsorbed base. The empty porcelain crucible was heated in an oven at 110 °C for 1 h, then cooled and weighed (W_1). A sample of 0.1 g was put into a porcelain crucible and then heated at 110 °C for 1 h and weighed (W_2). Samples in heated porcelain were put into a desiccator and then vacuumed. Next, ammonia gas was introduced to the desiccator until the gas saturated the desiccator. After completion, the desiccator was opened and allowed to run for about 30 min to remove residual ammonia that was not adsorbed. Next, the porcelain crucible containing the sample and absorbing ammonia was weighed (W_3). Calculation of total acidity using Eq. (1).

$$\text{Acidity} = \frac{(W_3 - W_2)}{(W_2 - W_1)M} \quad (1)$$

where, W_1 = weight of empty porcelain crucible after heating (g); W_2 = weight of porcelain crucible + sample after heating (g); W_3 = weight of porcelain crucible + sample after ammonia adsorption (g); M = molecular weight of NH_3 (g/mol).

Analysis using FTIR was conducted to verify the ammonia adsorbed on the material catalyst.

Catalytic activity test

The hydrocracking process was carried out in a semi-batch reactor, in which the catalyst and feed were put into one reactor but not mixed. The reactor was a stainless-steel column. A total of 10 g coconut oil feed was put into the column reactor, then 0.2 g of catalyst was placed in a container and put in the same column reactor. The catalyst/feed ratio was 2% (weight). The reactor column was inserted into a furnace made of stainless-steel coated ceramic and heated to 475 °C at a rate of 10 °C/min with a reaction time of three hours. During the reaction, hydrogen gas flowed to the reactor at a rate of 10 mL/min. The product was streamed through a stainless-steel pipe connected to a silicone hose and passed through a glass condenser. The liquid products were collected in an Erlenmeyer flask, then weighed (as the mass of the liquid product). Coke mass was the catalyst's weight after the hydrocracking sample subtracted the weight of the initial catalyst. The residual mass was the weight of residual feed in the reactor that was not converted. Gas mass was the weight of the initial feed subtracted by the weight (residue + coke + liquid). The determination of the catalytic activity of the catalyst follows Eq. (2) to Eq. (5).

$$\%\text{Liquid conversion} = \frac{\text{mass of the liquid}}{\text{mass of feed}} \times 100\% \quad (2)$$

$$\%\text{Coke conversion} = \frac{\text{mass of coke}}{\text{mass of feed}} \times 100\% \quad (3)$$

$$\%\text{Gas conversion} = \frac{\text{mass of the gas}}{\text{mass of feed}} \times 100\% \quad (4)$$

$$\%\text{Total conversion} = \frac{\text{mass of (liquid + gas + coke)}}{\text{mass of feed}} \times 100\% \quad (5)$$

Furthermore, the determination of liquid composition was conducted using Gas Chromatography-Mass Spectrometer (GC-MS). The percentage of the C_4–C_9 fraction was obtained by adding up the total area of the C_4–C_9 component in the chromatogram, then divided by the total chromatogram area of each sample. Likewise, the calculation of the percentage of the C_{10}–C_{15} fraction (bioavtur) was determined in the same procedure by changing C_4–C_9 to C_{10}–C_{15}. The percentage fraction was calculated using Eq. (6) and Eq. (7). The fraction peak area in the chromatogram was applied to calculate selectivity using Eq. (8).

$$\%C_4 - C_9 \text{ fraction} = \frac{\%\text{GC area of } C_4 - C_9 \text{ fraction}}{\%\text{ total GC area}} \times 100\% \quad (6)$$

$$\%\ C_{10}\text{-}C_{15} \text{ fraction} = \frac{\%\text{ GC area of } C_{10}\text{-}C_{15} \text{ fraction}}{\%\text{ total GC area}} \times 100\% \quad (7)$$

$$\%\text{ selectivity} = \frac{\%\text{ GC area bioavtur fraction}}{\%\text{ total GC area}} \times \%\text{ conversion of liquid} \quad (8)$$

■ RESULTS AND DISCUSSION

Characteristics of Silica-Rich Sodalite Zeolite Catalysts

Fig. 1 shows the FTIR spectra of the catalysts. According to Mofrad et al. [26], the typical absorption of sodalite is at the peak of 436, 467, 669, 711, 736, 867, and 988 cm^{-1}. In this study, all catalysts showed absorption

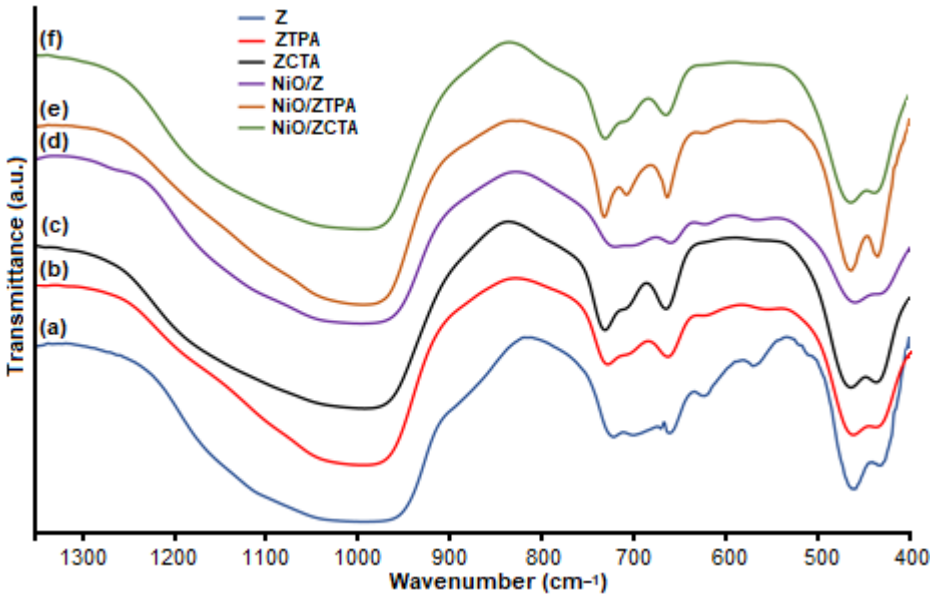

Fig 1. FTIR spectra of the silica-rich sodalite zeolite catalysts (a) without template (Z), (b) with CTAB (Z-CTA) and (c) with TPAB (Z-TPA) (d) NiO/Z (e) NiO/ZTPA (f) NiO/ZCTA

bands in the sodalite zeolite fingerprint area, which are 429–434 cm^{-1} as S4R bending vibrations, 459–467 cm^{-1} as O–T–O bending vibration, 660–664 cm^{-1} as T–O symmetrical stretching vibrations, 697, 722, and 978–992 cm^{-1} as T–O–T asymmetric stretching vibrations [27-28].

Asymmetrical T–O–T stretching vibration absorption was shifted at a higher wavenumber on the ZTPA and ZCTA catalyst when it was compared to Z. The same thing happened with NiO/ZTPA and NiO/ZCTA catalysts compared to NiO/Z. The wavenumber shift occurred from 978 cm^{-1} on Z to 983 cm^{-1} on ZTPA and 988 cm^{-1} on ZCTA. Whereas after impregnation with NiO, the wavenumber shift occurred from 991 cm^{-1} for NiO/Z to 996 cm^{-1} and 997 cm^{-1} for NiO/ZTPA and NiO/ZCTA, respectively. The shift of the absorption of the wave number in the higher direction indicates the vibration of Si–O–Al or Si–O–Si towards the lower energy. This is presumably because of adding TPA and CTA templates when forming a silica-rich sodalite framework causing longer bond distances. Besides, the asymmetric stretching vibration absorption band of T–O–T in the area experienced an increase in absorption intensity and downsizing of ZTPA, ZCTA, NiO/ZTPA, and NiO/ZCTA catalysts. According to Eterigho-Ikelegbe et al. [29], high intensity absorption in the fingerprint area of the main framework (not a wide peak) is preferred because it shows the catalyst has a more crystalline structure.

The XRD patterns of silica-rich zeolites are shown in Fig. 2. The characteristic peaks of the structures were determined based on the XRD standard patterns, which were taken from ICDD (International Center of Diffraction Database) or RUFF ID. The XRD patterns of the samples in Fig. 2 are relatively similar to the XRD standard pattern of sodalite zeolite based on RRUFF ID R040141 or ICDD.

Fig. 2 and Table 1 show that the XRD peaks of silica-rich sodalite zeolites from this study are like the previous results reported by Manique et al. [30], who synthesized sodalite through hydrothermal methods. In addition, the prominent data 2θ peak in the sample also complies with JCPDS 75-0709 and RRUFF ID R040141. These results indicate that all synthesis processes successfully produced sodalite. This material is called silica-rich sodalite zeolite because of its high Si content in its structure. These results also show that the addition of template treatment does not give a significant difference on the crystal structure of the resulting sodalites.

When aluminate and silicate interact under alkaline conditions, the Si–O–Si or Si–O–Al zeolite framework is formed, depending on the ratio of silicate

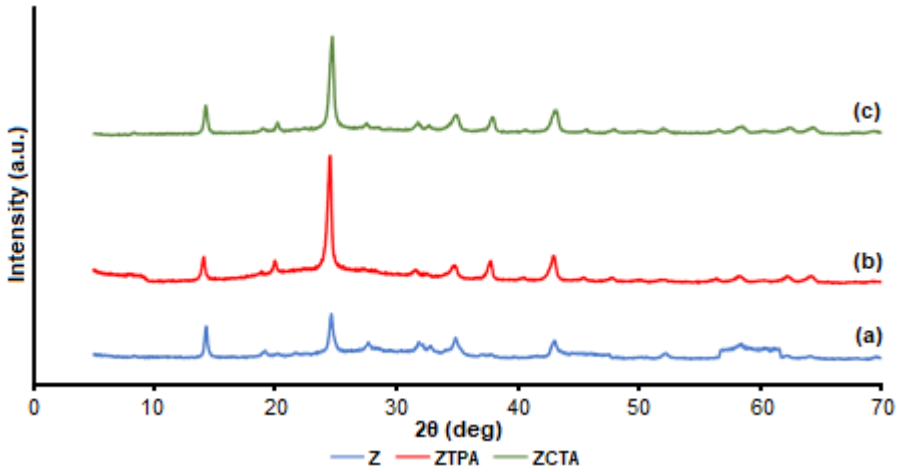

Fig 2. The powder XRD patterns of silica-rich sodalite zeolite (a) without template (Z), (b) with CTAB (Z-CTA) and (c) with TPAB (Z-TPA)

Table 1. Comparison of 2θ (°) between silica-rich sodalite zeolite and sodalite reference RRUFF ID No. R040141 and JCPDS No. 75-0709

Sodalite Reference 2θ (°) on		Sample 2θ (°)		
RRUFF ID R040141	JCPDS 75-0709	Z	ZTPA	ZCTA
14.16	14.1	14.31	14.26	14.11
24.66	24.5	24.65	24.71	24.54
31.99	31.8	31.87	31.79	31.62
35.13	35.0	34.89	34.94	34.79
	37.8	37.20	37.93	37.76
43.39	43.2	43.02	43.15	43.02

and aluminate [31]. The higher the Si/Al ratio, the more Si–O–Si will be formed, resulting in silica-rich sodalite zeolites. The hydrophobicity of silica-rich zeolite is a favorable character for interactions with organic compounds [8]. Hydrophobicity (zeolite-water interactions) in zeolites is primarily influenced by the chemical composition of zeolites, especially the Si/Al ratio. Zeolites with a high Si/Al ratio tend to have more hydrophobic character [32-33]. Bolis et al. [34] proposed that water molecules interact with the Al site of the zeolite framework. The few Si–OH species also influence hydrophobicity because Si–OH species can absorb water by forming stable bonds. Zeolites with the same framework type, their hydrophobicity increases with decreasing aluminum content, so zeolites with a higher Si/Al ratio will be more hydrophobic. This character is suitable for interacting with the raw material for coconut oil, which is also hydrophobic. The efficiency of the interaction of organic substances, in this case, coconut oil by high silica zeolites, depends on the interaction of organic substances with zeolites. And this is influenced by the structure, surface hydrophobicity, and adsorption sites of high silica zeolites and the character of organic materials [8].

Fig. 2 also shows that the use of templates slightly increases crystallinity. These results are in line with research by [25], who reported that the use of different templates produced different sodalite crystallinity. The use of different templates, CTAB and TPAB, from quaternary ammonium surfactants, is an important factor in the formation of different silicate species from dimers to 4-rings (4R) and the final sodalite zeolite structure [35] in basic conditions. A study conducted by Pavlova et al. [35] showed that the activation barrier of dimerization increased with TPA^+.

CTAB and TPAB are surface-active agents that work to reduce the surface tension of the liquid. Active

properties are obtained from the dual nature of the molecules. TPAB and CTAB surfactants were selected as pore-forming templates. Both have differences in the head and tail, although the part of heads has the same type of quaternary ammonium, but different tail shapes give different results. Several studies report the role of surfactant-templating that produces different pores in the zeolite [36], and pore size depending on the type of surfactants [37]. The effects of using templates and NiO loading on silica-rich sodalite zeolite pores and surfaces are given in Fig. 3 and Table 2.

Fig. 3(a) presents the adsorption isotherm patterns for samples Z, ZTPA, and ZCTA, which are classified as type IV according to the IUPAC adsorption isotherm classification [38]. Type IV isotherms signify mesoporous material. All three samples show a similar pattern of adsorption isotherms, where there was small amount of nitrogen molecular adsorption at the relative pressure P/P_0 = 0–0.7. An increase in the volume of absorbed nitrogen was observed at $P/P_0 > 0.7$. An increased volume of adsorbed nitrogen molecules indicates mesoporous filling, where the surface of the solid is covered by nitrogen molecules to form a single layer. The slope shows that the first multilayer has formed. The presence of pores on the surface of solid limits the number of layers on the adsorbate, resulting in capillary condensation. This capillary condensation causes hysteresis. The sample follows an H3 type hysteresis loop where the adsorption properties are not limited to high P/P_0. H3 type loops are observed because the aggregate of particles such as plates giving rise to pore-shaped slits [39] produces a narrow distribution of pore bodies with a wide neck size distribution [40]. ZTPA provides high absorption of nitrogen gas, which indicates that the pore volume in ZTPA is higher. These results indicate that the use of TPA has successfully enlarged pores, compared to zeolite without a template. However, an anomaly occurred in ZCTA samples, which showed small adsorption. It is estimated that the low nitrogen gas absorbed was caused by imperfect calcination, where many unburned CTA templates were still in the pore. This, in turn, caused pore closure.

On the other hand, Fig. 3(b) shows that the three samples give a similar form of adsorption isotherm with almost the same volume of nitrogen gas. This indicates that the NiO impregnation process in Z, ZTPA, and ZCTA samples produced almost the same pore and surface characteristics. The increase in the volume of nitrogen gas absorbed by NiO/ZCTA is due to the continued calcination process after the impregnation of Ni^{2+}, which burns the remains of the template. In samples of NiO/Z, NiO/ZTPA, and NiO/ZCTA, type H3 loop hysteresis occurs at a relative pressure of P/P_0 = 0.7–1. Hysteresis occurs as, at the same relative pressure P/P_0, the number of desorption of nitrogen adsorbed on the solid is lower than the number of adsorbed nitrogen molecules. This shows that the amount of adsorbate (N_2) remaining in the pore during desorption is high, indicating the number of mesoporous structures in the sample.

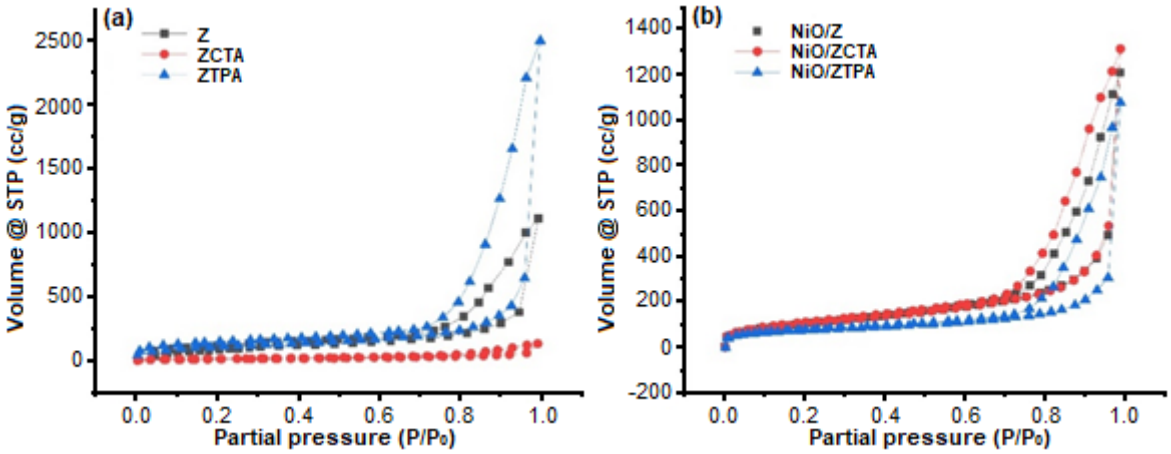

Fig 3. Isotherm adsorption of silica-rich sodalite zeolite (a) effects of template (b) effects of NiO loading

The critical micelle concentration (CMC) of CTAB is 9.2×10^{-4} M at 25 °C [41], whereas CMC of TPAB is 10^{-3} M and the solubility of TPAB at 20 °C > 1000 g/L in H_2O [42]. The addition of surfactant in sodium aluminate solution caused a decrease in the solution's surface tension. After reaching a certain concentration, the surface tension will be constant even though the surfactant concentration increases [43]. There is a difference in the length of the alkyl chain (tail), so the size of micelles will be different. Therefore, sodalite zeolites have different pore sizes. The length of the alkyl chain on CTAB is longer than TPAB; the longest CTAB chain contains 16 carbon, while TPAB only contains three carbon. Goyal et al. [44] reported that CTA^+ micelle diameters range from 130 to 210 Å. In contrast, according to Thapa et al. [45], TPA^+ micelle diameter about 13 Å. The larger CTA^+ micelle diameter from TPA^+ becomes the rationale for why the volume and surface area of ZCTA is higher than ZTPA, as shown in Fig. 4.

Fig. 4 presents the surface area, pore size, and total pore volume of synthesized silica-rich sodalite zeolites and NiO impregnated zeolites. The data shows that after impregnation by NiO, the surface area and pore volume of zeolite are significantly reduced, except Z, whose surface area and pore volume increase. Increased surface area and pore volume of Z may be caused by NiO placement on Z, which is more evenly distributed and does not form aggregates so that it does not clog pores. Therefore, the presence of NiO particles present on the surface of Z increases the surface area. On the other hand, the decrease in surface area on NiO/ZTPA and NiO/ZCTA is easily understood as a result of surface closure by NiO. The presence of carbon from incomplete combustion residues might accelerate pore aggregation. It may also be caused by the dispersion of NiO particles into the zeolite sodalite pores non-uniformly. This results in mouth obstruction of the porous channels and the outer surface of zeolites. For all silica-rich sodalite zeolite, the pore radius is almost the same and does not significantly change after NiO's impregnation. This indicates that the thickness of the NiO layer is much lower than the pore radius. All these results indicate that NiO particles were successfully impregnated on the surface and pore of silica-rich sodalite [24].

Metal loading increases the Brønsted and Lewis acid sites [46] as total acidity, as given in Table 2. It is hoped that more acid sites interact with the feed. Adsorption of ammonia base occurs through interactions with protons,

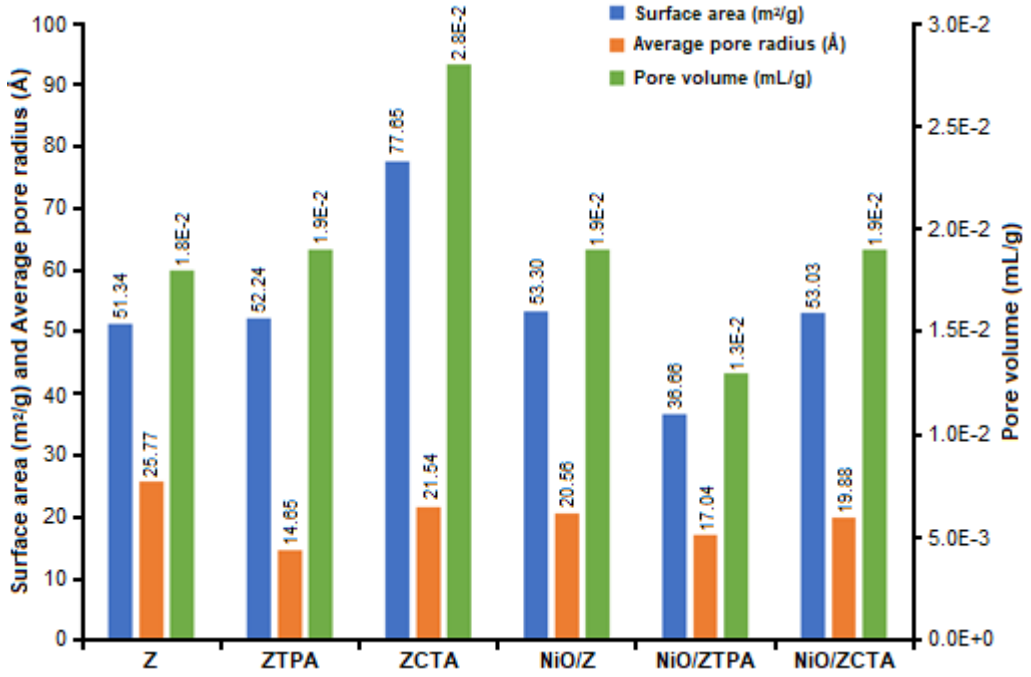

Fig 4. Surface area, pore diameter, and volume of synthesized silica-rich sodalite zeolites

Table 2. Total acidity of the catalyst

Catalyst Code	Acidity (mmol/g)
Silica-rich sodalite zeolite without template (Z)	7.9
Silica-rich sodalite zeolite - TPAB (ZTPA)	8.2
Silica-rich sodalite zeolite - CTAB (ZCTA)	11.4
NiO/Z	11.2
NiO/ZTPA	11.5
NiO/ZCTA	17.2

which are Brønsted acid sites or by receiving electron pairs from nitrogen atoms in ammonia where the catalyst acts as Lewis acid. In this data, it is known that an increase in acidity occurs when the preparation of a silica-rich zeolite catalyst support was carried out using a surfactant as a template. Total acidity increased by 3.79 and 44.30% in ZTPA and ZCTA, respectively.

The higher acidity value in ZCTA may be due to the greater surface area, as presented in Fig. 4 so that acidic sites are available on the surface. The addition of NiO significantly increases acidity. Ni metals from NiO are spread on the surface and in the pores. Moreover, silica-rich sodalite zeolite have empty orbitals that can accept electron pairs from the ammonia base [47]. NiO/Z acidity increased by 41.77% from Z, NiO/ZTPA increased by 40.24% from ZTPA, and NiO/ZCTA increased by 50.87% from ZCTA. Meanwhile, when compared to the catalyst without a template (Z), NiO/ZTPA acidity increased by 45.56%, and NiO/ZCTA increased by 117.7%. There is a correlation between total acidity and surface area and pore volume, wherewith increasing surface area and pore volume in Z, ZCTA, and ZTPA, acidity increases. This indicates that NiO is evenly distributed in line with surface area and pore volume.

Amorphous aluminosilicates formed at the beginning of zeolite preparations have many Lewis acid sites and several Brønsted acid sites. This is because Brønsted acid sites develop more on the surface of zeolites when well-defined crystals are formed [48]. The FTIR spectra in Fig. 5 show some firm absorption peaks at a wavenumber of 1635–1640 cm^{-1} on almost all catalysts, which are characteristic for ammonia bonding with Lewis acid sites [49]. It can be noted that there is not much difference at the peak of 1636 cm^{-1}, which indicates that the interaction of ammonia with Lewis acid sites is weak and does not depend on the zeolite structure and the amount of NiO added. In comparison, peaks at 1430–1450 cm^{-1} show ammonia interactions with

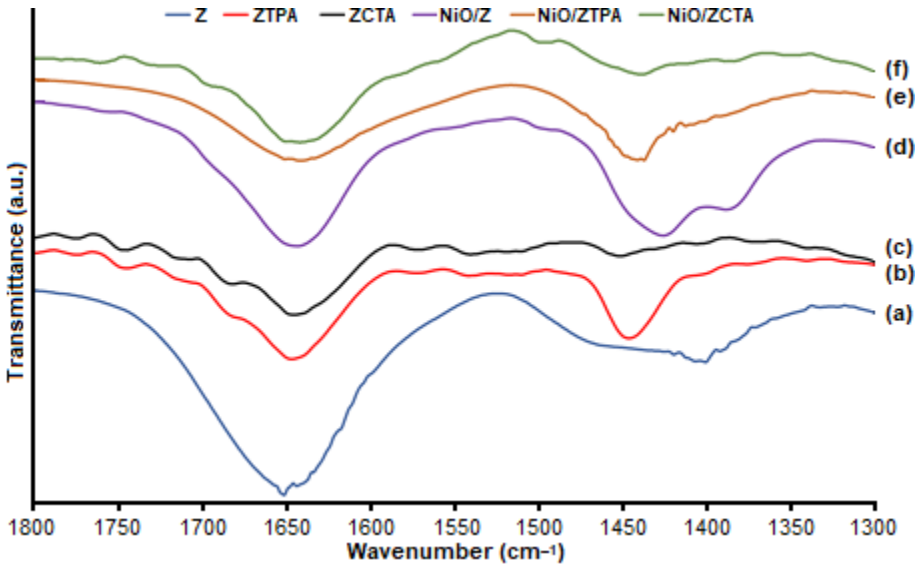

Fig 5. FTIR spectra of the catalysts after acidity test

Brønsted acid sites [50]. Unfortunately, in this area, absorption presents a very irregular form and overlaps with several other sub-bands. According to Barzetti [50], peaks in this area originate from ammonia decomposition into NH and NH_2^-. The effect of the addition of surfactants and NiO on Brønsted acid sites is difficult to explain. It can only be concluded that all catalysts have active Lewis and Brønsted acid sites.

Hydrocracking of Coconut Oil

Fig. 6 shows the effect of the addition of surfactants and NiO on the total conversion and composition of the coconut oil hydrocracking results after the hydrocracking process at 475 °C for 180 min, hydrogen flow rate of 10 mL/min, catalyst concentration of 2% to the feed.

The role of the templates TPA and CTA created catalyst porosity because, in hydrocracking, the porosity network was susceptible to the diffusion of unrestricted reactants and the resulting product. Besides, based on the data in Table 2, the presence of a template could increase the acidity. This case accorded with the report of Emdadi et al. [51]. The acidity and porosity of catalysts were significant; the acid sites of catalysts could effectively consume intermediates to form aiming products. Meanwhile, the porosities and cavities of catalysts could mediate the molecular sizes and structures of products [52].

Fig. 6 shows that the use of CTAB and TPAB templates in the formation of ZTPA and ZCTA silica-rich sodalite zeolite pores influences the increase in gas fraction yield. This is due to the specific pore size and shape as in the data in Fig. 4 where ZTPA and ZCTA have smaller pore sizes than Z, so that the catalyst is more selective than before to produce short-chain gas or hydrocarbon fractions. On the other hand, impregnation with NiO on NiO/Z, NiO/ZTPA, and NiO/ZCTA catalysts significantly rises liquid products. This is in accordance with Vichaphund et al. [53] report that the addition of metals is expected to modify the acidic properties and texture of the supporting material to promote cracking activity in terms of removing oxygenated compounds and increasing the number of hydrocarbons. It can be said that the role of nickel oxide as an active site is crucial. Fig. 6 also presents a catalytic activity for converting triglycerides into products consisting of liquid, gas, and coke. However, there is no significant difference in residue and coke due to the addition of surfactant and NiO treatment.

A total conversion is only slightly affected by the size and shape of the pores caused using templates and the loading of nickel oxide. Total conversions ranged from 70–86%, which did not show a significant difference. So, it can be concluded that the combination of the acidity of the catalyst and the accessibility of acid sites is an essential factor in the catalyst activity [54] towards the conversion of triglycerides in coconut oil.

Fig. 7(a) shows the catalyst effect on the composition of liquid product components from the hydrocracking process. The compounds presented in the liquid products are grouped into n-paraffin, consisting of biogasoline (C_4–C_9) and bioavtur hydrocarbon range (C_{10}–C_{15}). Both fractions are n-paraffin compounds that

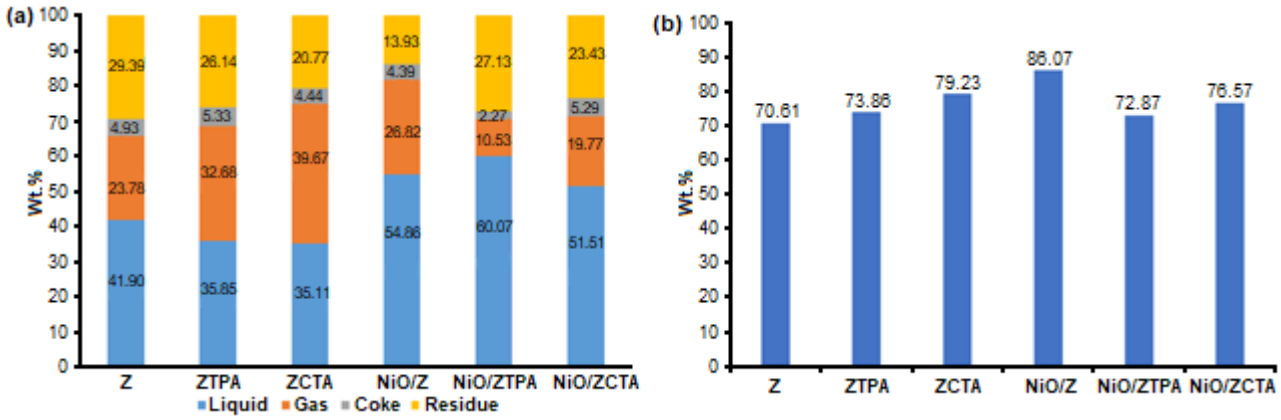

Fig 6. The effect of templates and NiO on (a) type of hydrocracking products and (b) total conversion

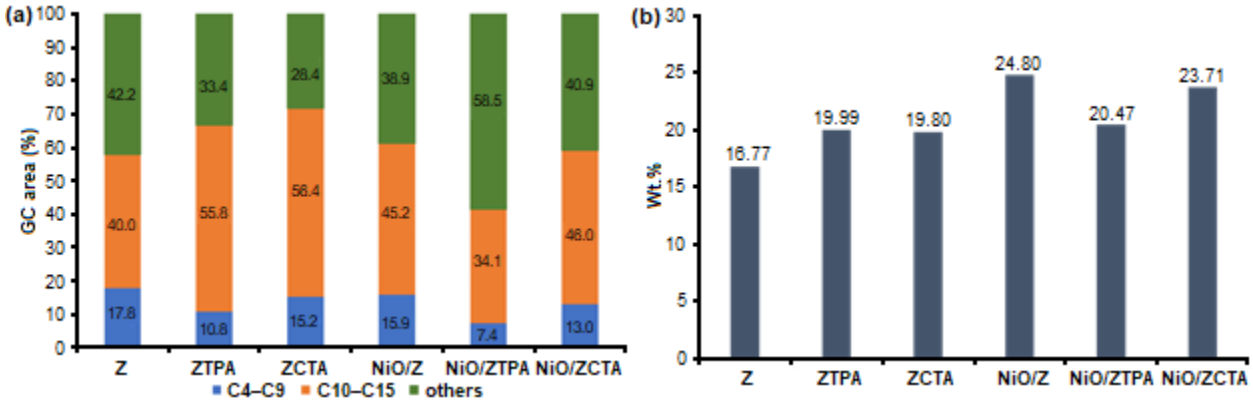

Fig 7. Effect of catalysts on (a) the composition of liquid products (b) The percentage of bioavtur fraction (C_{10}-C_{15}) selectivity

are produced in the hydrocracking reaction at temperature of 475 °C. According to Li et al. [55], paraffin is formed through decarboxylation and decarbonylation reactions. Fig. 7(a) also shows that the hydrocracking process also produces other products such as alkenes, carboxylic acids, ethers, alcohols, etc. with a percentage of 30–40% except for NiO/ZTPA which is 58.54%. The percentage of bioavtur fuel fraction increased in the ZTPA and ZCTA catalysts. This data shows the TPA and CTA templates are significant in increasing the bioavtur fraction.

The role of templates in enhancing bioavtur products is by increasing the ability of the feeds (triglycerides) to diffuse into the pores and active sites of the catalyst. Based on Fig. 4, catalysts with TPA and CTA templates have more pores than without templates. Pores and cavities produce more active sites. Therefore, more triglycerides were able to diffuse and interact with active sites and in cavities of a specific size and shape, thus producing short and long-chain hydrocarbon products. The C_4-C_9 short-chain hydrocarbon fraction was produced in smaller quantities than C_{10}–C_{15}, probably due to the lighter fraction being faster. At the same time, the presence of many pores allows the reaction to be retained in the cavity to produce a longer carbon chain.

Fig. 7(a) shows the ability of the catalyst to produce bioavtur fractions after impregnation with NiO seems to decrease, except Z, which is impregnated into NiO/Z. The surface area of NiO/Z is relatively higher than NiO/ZTPA and NiO/ZCTA. Therefore, it has a higher ability to produce bioavtur. The increase in product selectivity obtained from catalysts containing NiO can be observed in Fig. 7(b). It appears that the addition of NiO does not provide more selective results on biogasoline and bioavtur products.

The high yield in the liquid products in Fig. 6 and selectivity performed by catalysts in Fig. 7 are due to their pore size and shape of the catalysts and the easiness of NiO loading. The fact indicated the incorporation of nickel oxide into Z, ZTPA, and ZCTA catalysts depict a bifunctional character consisting of acid and metal sites in agreement with Xu et al. [56]. The acidity properties of zeolites indicated their catalytic potential for various hydrocarbon reactions.

■ CONCLUSION

The CTAB surfactant as a template was able to increase the surface area of the catalyst from 51.338 m^2/g in silica-rich zeolites without surfactants (Z) to 77.653 m^2/g on the CTAB template (ZCTA). However, it did not occur in the TPAB template (ZTPA). The use of templates slightly increased the acidity of the catalysts from 7.9 mmol/g to 8.2 mmol/g on ZTPA and 11.4 mmol/g on ZCTA. The addition of NiO on catalysts also improved the acidity property. The highest acidity was 17.2 mmol/g in the NiO/ZCTA sample.

NiO/silica-rich sodalite zeolites in the hydrocracking process resulted in gas products when the surface area was greater, namely 23.781, 32.68, and 39.673% for Z, ZTPA, and ZCTA, respectively. The

presence of NiO increased liquid products and selectivity of bioavtur fraction (C_{10}–C_{15}), where the highest percentage of liquid obtained was 60.07% from NiO/ZTPA.

■ ACKNOWLEDGMENTS

The authors would like gratefully to acknowledge to the Directorate General of Research and Development, the Ministry of Research, Technology, and Higher Education of Indonesia, for financial support in the 2019 fiscal year with the grant number 101-27/UN7.P4.3/PP/2019. The authors would like to extend the gratitude to our research team, i.e., R. Kurniasari and R. Kurniawati, for the support during the experiments.

■ REFERENCES

[1] Esaifan, M., Warr, L.N., Grathoff, G., Meyer, T., Schafmeister, M.T., Kruth, A., and Testrich, H., 2019, Synthesis of hydroxy-sodalite/cancrinite zeolites from calcite-bearing kaolin for the removal of heavy metal ions in aqueous media, *Minerals*, 9, 484.

[2] Buhl, J.C., 2016, Enhanced methods of crystallization: The crossover synthesis from gel to melt flow - A case study on sodalites, *Microporous Mesoporous Mater.*, 236, 13–20.

[3] Dey, K.P., Ghosh, S., and Naskar, M.K., 2013, Organic template-free synthesis of ZSM-5 zeolite particles using rice husk ash as silica source, *Ceram. Int.*, 39 (2), 2153–2157.

[4] Sriatun, S., Taslimah, T., Cahyo, E.N., and Saputro, F.D., 2017, Sintesis dan karakterisasi zeolit Y, *JKSA*, 20 (1), 19–24.

[5] Sriatun, S., Taslimah, T., and Suyati, L., 2018, Synthesis of zeolite from sugarcane bagasse ash using cetyltrimethylammonium bromide as structure directing agent, *Indones. J. Chem.*, 18 (1), 159–165.

[6] Wang, L., Lei, H., Bu, Q., Ren, S., Wei, Y., Zhu, L., Zhang, X., Liu, Y., Yadavalli, G., Lee, J., Chen, S., and Tang, J., 2014, Aromatic hydrocarbons production from ex situ catalysis of pyrolysis vapor over Zinc modified ZSM-5 in a packed-bed catalysis coupled with microwave pyrolysis reactor, *Fuel*, 129, 78–85.

[7] Jo, D., Ryu, T., Park, G.T., Kim, P.S., Kim, C.H., Nam, I.S., and Hong, S.B., 2016, Synthesis of high-silica LTA and UFI zeolites and NH_3–SCR performance of their copper-exchanged form, *ACS Catal.*, 6 (4), 2443–2447.

[8] Jiang, N., Shang, R., Heijman, S.G.J., and Rietveld, L.C., 2018, High-silica zeolites for adsorption of organic micro-pollutants in water treatment: A review, *Water Res.*, 144, 145–161.

[9] Gao, Y., Zheng, B., Wu, G., Ma, F., and Liu, C., 2016, Effect of the Si/Al ratio on the performance of hierarchical ZSM-5 zeolites for methanol aromatization, *RSC Adv.*, 6 (87), 83581–83588.

[10] Smirniotis, P.G., and Zhang, W., 1996, Effect of the Si/Al ratio and of the zeolite structure on the performance of dealuminated zeolites for the reforming of hydrocarbon mixtures, *Ind. Eng. Chem. Res.*, 35 (9), 3055–3066.

[11] Shvets, O.V., Kasian, N., Zukal, A., Pinkas, J., and Čejka, J., 2010, The role of template structure and synergism between inorganic and organic structure directing agents in the synthesis of UTL zeolite, *Chem. Mater.*, 22 (11), 3482–3495.

[12] Sriatun, S., Taslimah, T., and Suyati, 2015, Pemanfaatan katalis silika alumina dari bagasse pada pembuatan biodiesel dari minyak goreng sisa pakai, *Jurnal Teknologi Industri Pertanian*, 25 (1), 35–42.

[13] Abbasov, V.M., Ibrahimov, H.C., Mukhtarova, G.S., and Abdullayev, E., 2016, Acid treated halloysite clay nanotubes as catalyst supports for fuel production by catalytic hydrocracking of heavy crude oil, *Fuel*, 184, 555–558.

[14] Romero, M.J.A., Pizzi, A., Toscano, G., Busca, G., Bosio, B., and Arato, E., 2016, Deoxygenation of waste cooking oil and non-edible oil for the production of liquid hydrocarbon biofuels, *Waste Manage.*, 47, 62–68.

[15] Vonortas, A., Kubička, D., and Papayannakos, N., 2014, Catalytic co-hydroprocessing of gasoil–palm oil/AVO mixtures over a NiMo/γ-Al_2O_3 catalyst, *Fuel*, 116, 49–55.

[16] Hanaoka, T., Miyazawa, T., Shimura, K., and Hirata, S., 2015, Jet fuel synthesis in hydrocracking of Fischer–Tropsch product over Pt-loaded zeolite catalysts prepared using microemulsions, *Fuel Process. Technol.*, 129, 139–146.

[17] Yotsomnuk, P., and Skolpap, W., 2017, Biofuel production from waste virgin coconut oil by hydrocracking over HZSM-5 zeolite, *Int. J. Adv. Sci. Eng. Technol.*, 5 (2), 54–57.

[18] Tanzer, S.E., Posada, J., Geraedts, S., and Ramírez, A., 2019, Lignocellulosic marine biofuel: Technoeconomic and environmental assessment for production in Brazil and Sweden, *J. Cleaner Prod.*, 239, 117845.

[19] Liu, S., Zhu, Q., Guan, Q., He, L., and Li, W., 2015, Bio-aviation fuel production from hydroprocessing castor oil promoted by the nickel-based bifunctional catalysts, *Bioresour. Technol.*, 183, 93–100.

[20] Widiyadi, A., Guspiani, G.A., Riady, J., Andreanto, R., Chaiunnisa, S.D., and Widayat, W., 2018, Preparation and characterization of $NiMo/Al_2O_3$ catalyst for hydrocracking processing, *E3S Web Conf.*, 31, 03011.

[21] Eller, Z., Varga, Z., and Hancsók, J., 2016, Advanced production process of jet fuel components from technical grade coconut oil with special hydrocracking, *Fuel*, 182, 713–720.

[22] Al-Muttaqii, M., Kurniawansyah, F., Prajitno, D.H., and Roesyadi, A., 2019, Bio-kerosene and bio-gasoil from coconut oils via hydrocracking process over Ni-Fe/HZSM-5 catalyst, *Bull. Chem. React. Eng. Catal.*, 14 (2), 309–319.

[23] Widayat, W., Saputro, S.A., Ginting, E.M., Annisa, A.N., and Satriadi, H., 2017, Biofuel production by catalytic cracking method using Zn/HZSM-5 catalyst, *ARPN J. Eng. Appl. Sci.*, 12 (22), 6347–6351.

[24] Boateng, L., Ansong, R., Owusu, W., and Steiner-Asiedu, M., 2016, Coconut oil and palm oil's role in nutrition, health and national development: A review, *Ghana Med. J.*, 50 (3), 189–196.

[25] Lapari, S.S., Ramli, Z., and Triwahyono, S., 2015, Effect of different templates on the synthesis of mesoporous sodalite, *J. Chem.*, 2015, 272613.

[26] Mofrad, A.M., Schellenberg, P.S., Peixoto, C., Hunt, H.K., and Hammond, K.D., 2020, Calculated infrared and Raman signatures of Ag^+, Cd^{2+}, Pb^{2+}, Hg^{2+}, Ca^{2+}, Mg^{2+}, and K^+ sodalites, *Microporous Mesoporous Mater.*, 296, 109983.

[27] Song, Q., Shen, J., Yang, Y., Wang, J., Yang, Y., Sun, J., Jiang, B., and Liao, Z., 2020, Effect of temperature on the synthesis of sodalite by crystal transition process, *Microporous Mesoporous Mater.*, 292, 109755.

[28] Sari, M.E.F., Suprapto, S., and Prasetyoko, D., 2018, Direct synthesis of sodalite from kaolin: The influence of alkalinity, *Indones. J. Chem.*, 18 (4), 607–613.

[29] Eterigho-Ikelegbe, O., Bada, S., Daramola, M.O., and Falcon, R., 2020, Synthesis of high purity hydroxy sodalite nanoparticles via pore-plugging hydrothermal method for inorganic membrane development: Effect of synthesis variables on crystallinity, crystal size and morphology, *Mater. Today: Proc.*, In Press, Corrected Proof.

[30] Manique, M.C., Lacerda, L.V., Alves, A.K., and Bergmann, C.P., 2017, Biodiesel production using coal fly ash-derived sodalite as a heterogeneous catalyst, *Fuel*, 190, 268–273.

[31] Lutz, W., 2014, Zeolite Y: Synthesis, modification, and properties–A case revisited, *Adv. Mater. Sci. Eng.*, 2014, 724248.

[32] Güvenç, E., and Ahunbay, M.G., 2012, Adsorption of methyl tertiary butyl ether and trichloroethylene in MFI-type zeolites, *J. Phys. Chem. C*, 116 (41), 21836–21843.

[33] Grieco, S.A., and Ramarao, B.V., 2013, Removal of TCEP from aqueous solutions by adsorption with zeolites, *Colloids Surf., A*, 434, 329–338.

[34] Bolis, V., Busco, C., and Ugliengo, P., 2006, Thermodynamic study of water adsorption in high-silica zeolites, *J. Phys. Chem. B*, 110 (30), 14849–14859.

[35] Pavlova, A., Trinh, T.T., van Santen, R.A., and Meijer, E.J., 2013, Clarifying the role of sodium in the silica oligomerization reaction, *Phys. Chem. Chem. Phys.*, 15 (4), 1123–1129.

[36] Al-Ani, A., Haslam, J.J.C., Mordvinova, N.E., Lebedev, O.I., Vicente, A., Fernandez, C., and Zholobenko, V., 2019, Synthesis of nanostructured catalysts by surfactant-templating of large-pore zeolites, *Nanoscale Adv.*, 1 (5), 2029–2039.

[37] Cho, K., Na, K., Kim, J., Terasaki, O., and Ryoo, R., 2012, Zeolite synthesis using hierarchical structure-directing surfactants: Retaining porous structure of initial synthesis gel and precursors, *Chem. Mater.*, 24 (14), 2733–2738.

[38] Sotomayor, F.J., Cychosz, K.A., and Thommes, M., 2018, Characterization of micro/mesoporous materials by physisorption: concepts and case studies, *Acc. Mater. Surf. Res.*, 3 (2), 34–50.

[39] Yurdakal, S., Garlisi, C., Özcan, L., Bellardita, M., and Palmisano, G., 2019, "(Photo)catalyst characterization techniques: Adsorption isotherms and BET, SEM, FTIR, UV–Vis, photoluminescence, and electrochemical characterizations" in *Heterogeneous Photocatalysis: Relationships with Heterogeneous Catalysis and Perspectives*, Eds. Marcì, G., and Palmisano, L., Elsevier, 87–152.

[40] Cychosz, K.A., and Thommes, M., 2018, Progress in the physisorption characterization of nanoporous gas storage materials, *Engineering*, 4 (4), 559–566.

[41] Goronja, J.M., Janošević-Ležaić, A., Dimitrijević, B.M., Malenović, A., Stanisavljev, D., and Pejić, N., 2016, Determination of critical micelle concentration of cetyltrimethyl-ammonium bromide: Different procedures for analysis of experimental data, *Hem. Ind.*, 70 (4), 485–492.

[42] Steigman, J., Cohen, I., and Spingola, F., 1965, Micelle formation by a long-chain cation surfactant in aqueous solutions of the lower quaternary ammonium bromides, *J. Colloid Sci.*, 20 (7), 732–741.

[43] Vitagliano, V., D'Errico, G., Ortona, O., and Paduano, L., 2001, "Isothermal diffusion and intradiffusion in surfactant solutions" in: *Handbook of Surfaces and Interfaces of Materials: Biomolecules, Biointerfaces, and Applications*, Eds. Nalwa, H.S., Academic Press, Burlington, US, 545–611.

[44] Goyal, P.S., Dasannacharya, B.A., Kelkar, V.K., Manohar, C., Srinivasa Rao, K., and Valaulikar, B.S., 1991, Shapes and sizes of micelles in CTAB solutions, *Physica B*, 174 (1-4), 196–199.

[45] Thapa, U., Dey, J., Kumar, S., Hassan, P.A., Aswal, V.K., and Ismail, K., 2013, Tetraalkylammonium ion induced micelle-to-vesicle transition in aqueous sodium dioctylsulfosuccinate solutions, *Soft Matter*, 9 (47), 11225–11232.

[46] Trisunaryanti, W., Triyono, T., Armunanto, R., Hastuti, L.P., Ristiana, D.D., and Ginting, R.V., 2018, Hydrocracking of α-cellulose using Co, Ni, and Pd supported on mordenite catalysts, *Indones. J. Chem.*, 18 (1), 166–172.

[47] Efiyanti, L., and Trisunaryanti, W., 2014, Hidrorengkah katalitik minyak kulit biji jambu mete (CNSL) menjadi fraksi bensin dan diesel, *JPHH*, 32 (1), 71–81.

[48] Khan, G.M., Arafat, S.M.Y., Reza, M.N., Razzaque, S.M., and Alam, M., 2010, Linde Type-A zeolite synthesis and effect of crystallization on its surface acidity, *Indian J. Chem. Technol.*, 17, 303–308.

[49] Al Sofy, S.A.A., 2018, Fourier transformation infrared spectroscopic studies of acidity of NaH-13 X zeolites, *Al-Nahrain J. Eng. Sci.*, 21 (3), 428–435.

[50] Barzetti, T., Selli, E., Moscotti, D., and Forni, L., 1996, Pyridine and ammonia as probes for FTIR analysis of solid acid catalysts, *J. Chem. Soc., Faraday Trans.*, 92 (8), 1401–1407.

[51] Emdadi, L., Oh, S.C., Wu, Y., Oliaee, S.N., Diao, Y., Zhu, G., and Liu, D., 2016, The role of external acidity of meso-/microporous zeolites in determining selectivity for acid-catalyzed reactions of benzyl alcohol, *J. Catal.*, 335, 165–174.

[52] Jiao, W., Su, J., Zhou, H., Liu, S., Liu, C., Zhang, L., Wang, Y., and Yang, W., 2020, Dual template synthesis of SAPO-18/34 zeolite intergrowths and their performances in direct conversion of syngas to olefins, *Microporous Mesoporous Mater.*, 306, 110444.

[53] Vichaphund, S., Aht-ong, D., Sricharoenchaikul, V., and Atong, D., 2015, Production of aromatic compounds from catalytic fast pyrolysis of Jatropha residues using metal/HZSM-5 prepared by ion-exchange and impregnation methods, *Renewable Energy*, 79, 28–37.

[54] Socci, J., Saraeian, A., Stefanidis, S.D., Banks, S.W., Shanks, B.H., and Bridgwater, T., 2019, The role of catalyst acidity and shape selectivity on products from the catalytic fast pyrolysis of beech wood, *J. Anal. Appl. Pyrolysis*, In Press, Corrected Proof.

[55] Li, T., Cheng, J., Huang, R., Yang, W., Zhou, J., and Cen, K., 2016, Hydrocracking of palm oil to jet biofuel over different zeolites, *Int. J. Hydrogen Energy*, 41 (47), 21883–21887.

[56] Xu, W., Chen, B., Jiang, X., Xu, F., Chen, X., Chen, L., Wu, J., Fu, M., and Ye, D., 2020, Effect of calcium addition in plasma catalysis for toluene removal by Ni/ZSM-5: Acidity/basicity, catalytic activity and reaction mechanism, *J. Hazard. Mater.*, 387, 122004.